Water Repellent Periodic Mesoporous Organosilicas

Wendong Wang,[†] Daniel Grozea,[‡] Sandeep Kohli,[§] Douglas D. Perovic,[‡] and Geoffrey A. Ozin[†,*]

[†]Materials Chemistry Research Group, Department of Chemistry, University of Toronto, 80 St. George Street, Toronto, M5S 3H6, Canada, [‡]Department of Materials Science and Engineering, University of Toronto, 184 College Street, Toronto, Ontario, M5S 3E4 Canada, and [§]Department of Chemistry, Colorado State University, Fort Collins, Colorado 80523, United States

ABSTRACT This paper demonstrates for the first time thermally induced gradual hydrophobization, monitored quantitatively by ellipsometric porosimetry, of four prototypical periodic mesoporous organosilicas (PMOs) that are tailored through materials chemistry for use as low-dielectric-constant (low *k*) materials in microprocessors. Theoretical aspects of this quantification are briefly discussed. A comparison of structural, mechanical, dielectric, and hydrophobic properties of ethane, methane, ethene, and 3-ring PMOs is made. Particularly, ethane, methane, and 3-ring PMOs show impressive water repellency at post-treatment temperatures as low as 350 °C, with corresponding Young's modulus values greater than 10 GPa and *k* values smaller than 2, a figure of merit that satisfies the technological requirements of future generation microchips.

KEYWORDS: mesoporous materials · periodic mesoporous organosilica · ellipsometric porosimetry · water repellency · hybrid materials

Periodic mesoporous organosilica (PMO) is a new class of materials that possess ordered porous structure, uniform pore size of 2−30 nm and organic−inorganic hybrid pore walls.[1−5] The organic components give rise to a more hydrophobic environment inside the pores of PMOs than their pristine silica counterparts. This increased hydrophobicity provides fine-tuning of the host−guest interactions and benefits applications such as catalysis,[6] drug delivery,[7] protein refolding,[8] and separation.[9] In addition, it renders PMOs humidity resistant,[10,11] giving these materials an advantage for potential applications in nanoelectronics, solar cells, displays, and lighting.

Our group has reported the synthesis of PMO thin films for use as low-dielectric-constant (low-*k*) materials in microprocessors through solution phase spin-coating[11] and vapor phase vacuum-assisted aerosol-deposition,[12] and has shown that humidity resistance is one of the many attributes of PMOs that must be understood, controlled, and quantified for the development of a practical low-*k* material. Here for the first time we report how the gradual hydrophobization of PMO thin films can be commanded synthetically and quantitatively defined by ellipsometric porosimetry, a relatively new and convenient method that can be readily extended to other porous thin film materials, where assessing the hydrophobicity is critical for their respective applications.

Ellipsometric porosimetry (EP) is an analytical technique that fuses the power of thin films analysis by spectroscopic ellipsometry and the strength of porous materials analysis by adsorption porosimetry. It was first developed in response to the semiconductor industry's need for a nondestructive method to determine pore size, pore volume,[13,14] and Young's modulus[15] of porous low-*k* thin films. The adsorbates used in these early studies were volatile organic solvents such as toluene, heptanes, and carbon tetrachloride, and the analysis used a vacuum chamber with a vapor pressure control system. Sanchez and co-workers improved the EP system by using water as the adsorbate so that the analysis could be performed at ambient temperature and pressure.[16] Water does not wet most of the solid perfectly, so a contact angle needs to be included in the analysis of experimental data using the Kelvin equation:

$$\ln \frac{P}{P_0} = \frac{-2\gamma V \cos\theta}{rRT} \qquad (1)$$

where P/P_0 is the relative humidity, γ is the surface tension of water, V is the molar volume of water, θ is the contact angle of water on the surface of an adsorbent, r is the pore radius, R is the gas constant, and T is the temperature. Although the Kelvin equation is often used for calculating pore size distribution with the knowledge of contact angle values, the experiment can be inverted to deduce the value of a contact angle if pore size is known. This value provides information of the hydrophilic−hydrophobic character of a porous material, a pivotal piece of information for the development of a low dielectric constant material for

*Address correspondence to gozin@chem.utoronto.ca.

Received for review October 28, 2010 and accepted December 21, 2010.

Published online January 04, 2011
10.1021/nn102929t

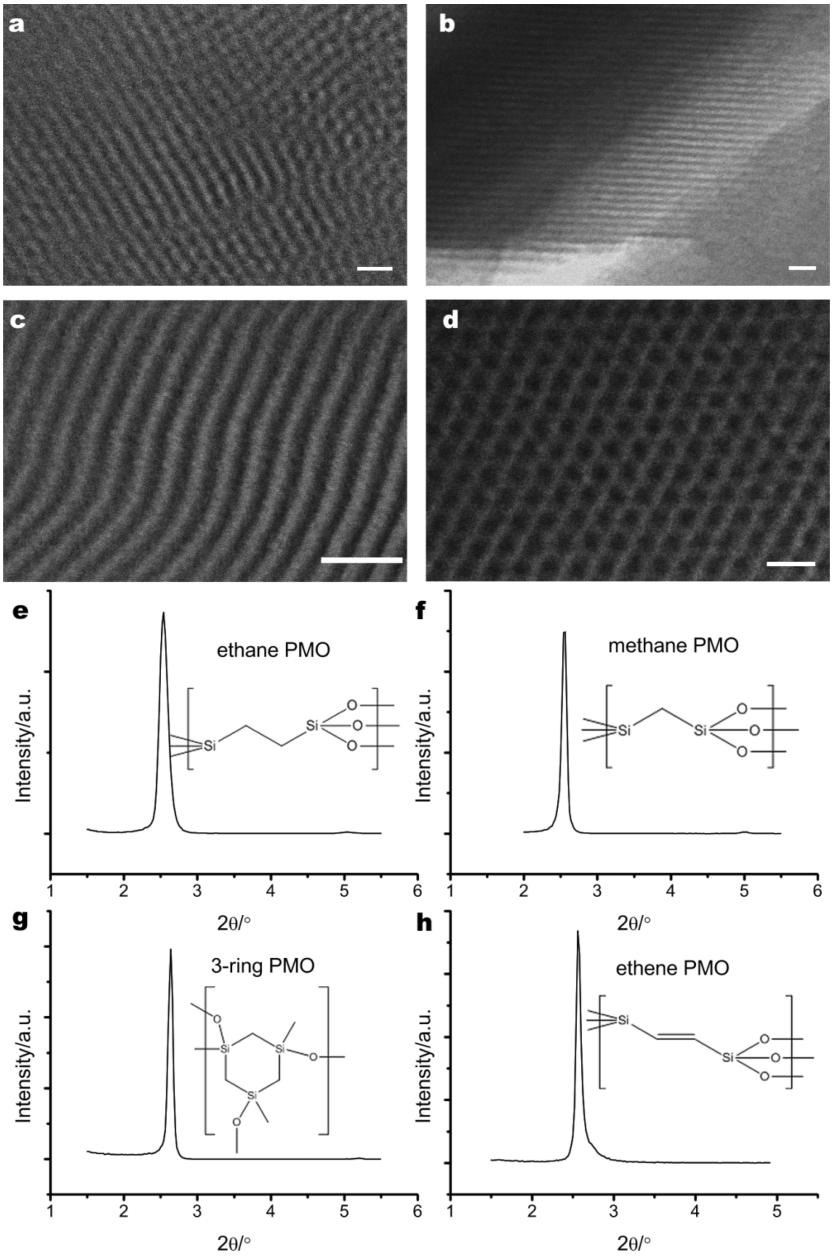

Figure 1. Representative TEM images of (a) ethane, (b) methane, (c) 3-ring and (d) ethene PMO, and the corresponding XRD patterns listed in the same order in panels e−h. Structural formulas of PMOs are drawn besides their XRD patterns.

microelectronic packaging applications and the central objective of this paper.

RESULTS AND DISCUSSION

Preparation of Thin Films of PMOs. The thin films of PMOs in this study were prepared by spin-coating. The precursors of the four PMOs (ethane, methane, ethene, and 3-ring PMOs) that we choose to investigate have relatively simple bridging groups and are commercially available and thus suitable for volume manufacturing. In fact, they have been recognized by the semiconductor industry as ideal candidates for the next generation of ultralow-*k* materials with *k* values of 2 and below.[17]

In a typical synthesis, a PMO precursor was added to a solution of cetyltrimethyl-ammonium chloride, hydrochloric acid, ethanol, and water. This solution was stirred at room temperature for 30 min to 2 h before being spin-coated onto a clean silicon wafer. The stirring time was critical to obtain good mesostructural ordering. The as-deposited films were then heated under nitrogen at 150 °C for 2 h before being washed by HCl in ethanol solution to remove surfactants. Films were heated again at 300 to 500 °C under nitrogen before characterization was undertaken. Figure 1 shows the transmission electron microscopy (TEM) images and XRD patterns, both indicating good mesostructural ordering of these thin films. The pore size estimated from TEM images is about 2 nm.

Often overlooked in quantitative studies of low-*k* materials is that great care should be taken not to

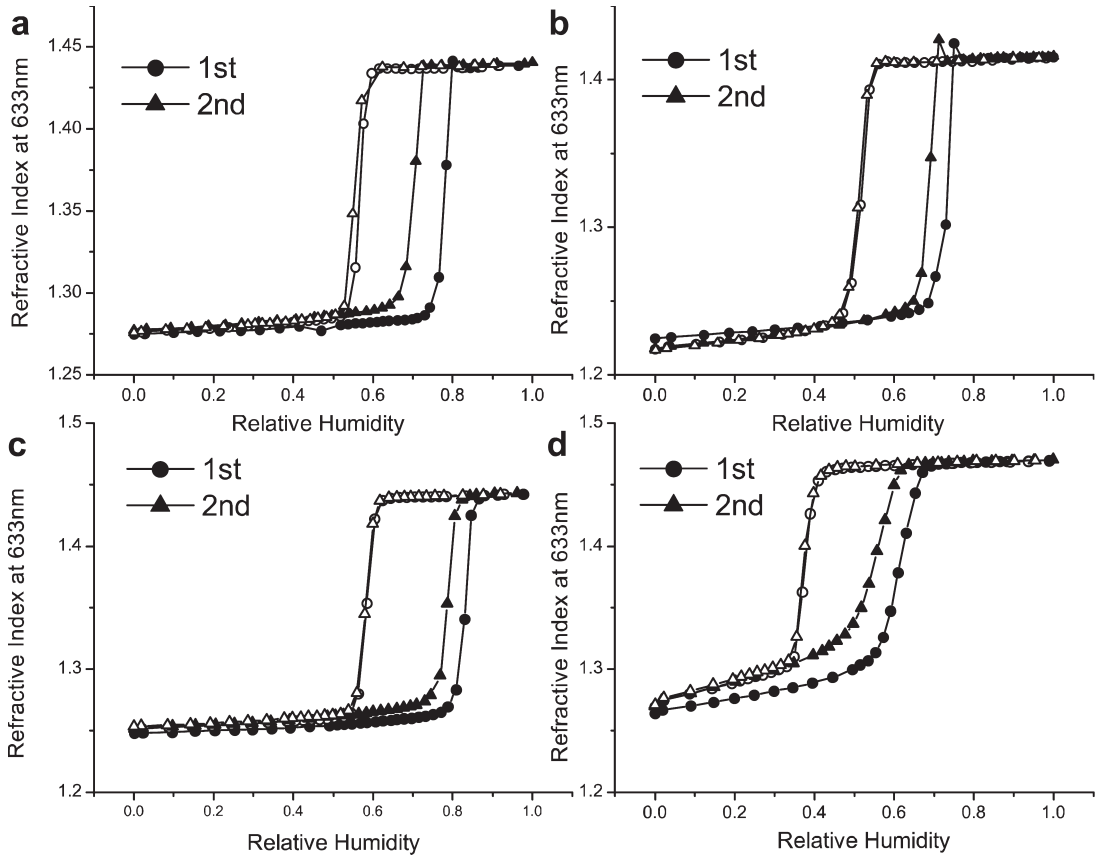

Figure 2. Isotherms of (a) ethane, (b) methane, (c) 3-ring, and (d) ethene PMO post-treated at 350 °C for 2 h. In each plot, filled symbols represent an adsorption branch and empty symbols represent a desorption branch. On each sample, two adsorption−desorption circles are measured. The circular shape corresponds to the first, and the triangular shape corresponds to the second.

introduce any organic contaminant during the washing and heating steps, because those contaminants will be deposited inside the pores and alter the hydrophilic−hydrophobic character of the pore surface. Another point of care is that moisture in air can also react with the pore surface, especially at elevated temperatures. To reduce the effect of moisture, the furnace tube containing samples was first evacuated and then refilled with dry nitrogen before any thermal treatment.

Characterization by Ellipsometric Porosimetry (EP). A typical EP measurement gives the change of refractive index and thickness of a thin film with respect to relative humidity (RH). The change of the refractive index relates quantitatively to the amount of water adsorbed inside mesopores, so the term isotherm is used to refer to the plots of refractive index *versus* relative humidity.[14] Figure 2 shows typical isotherms of four PMOs, each being measured twice. The sharp increase of the refractive index in an adsorption branch, which signals water condensation inside mesopores (pore condensation), occurs at a higher relative humidity in the first isotherm than in the second one. This difference is due to water rehydrolyzing the pore wall surface during the measurement. The sharp decrease of the refractive index in a desorption branch, which signals water evaporation from the mesopores (pore evaporation), occurs at the same relative humidity in the first and the second isotherm, suggesting the rehydrolysis is completed before the pore evaporation in the first measurement.

According to the Kelvin equation, the higher the relative humidity of the pore condensation is, the more hydrophobic the pore wall is. The sequence of hydrophobicity of all four PMOs post-treated at 350 °C is 3-ring (83%RH) > ethane (78%RH) > methane (73%) > ethene (61%RH). A subtle feature also related to the hydrophilic−hydrophobic character of the pore wall is the slope of an isotherm before pore condensation. This slope is higher in the second isotherm than in the first isotherm for all four PMOs. This difference is due to the rehydrolysis that occurs in the first absorption−desorption circle. Of all PMOs, the difference in the slopes of two isotherms is most pronounced in ethene PMO, indicating that ethene PMO is most susceptible to rehydrolysis. In addition, ethene PMO has the highest slope among all four PMOs, suggesting again that the pore wall of ethene PMO is the most hydrophilic.

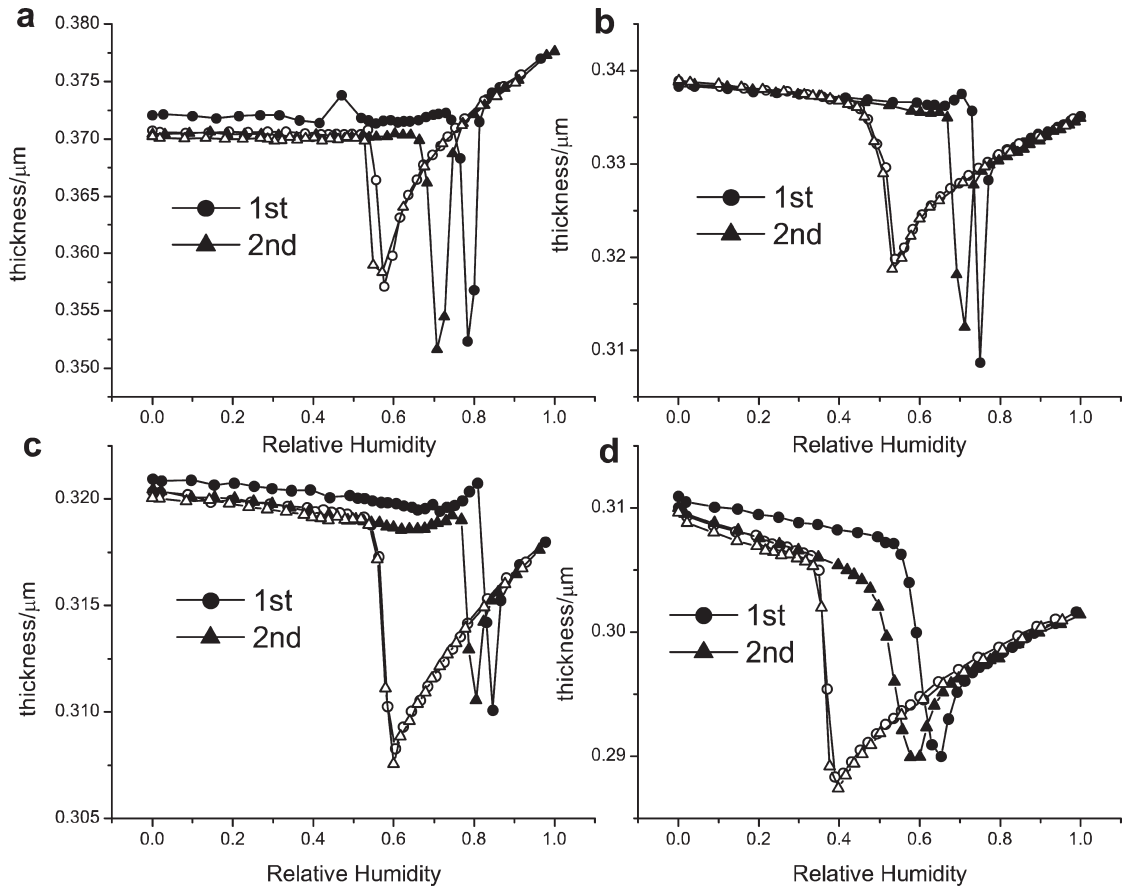

Figure 3. Changes of thickness with respect to relative humidity of the thin films of (a) ethane, (b) methane, (c) 3-ring, and (d) ethene PMO post-treated at 350 °C for 2 h.

The changes of thickness are plotted in Figure 3. Water condensation inside mesopores induces capillary pressure, which compresses the film and results in a decrease in thickness. All four PMOs show this decrease in thickness during capillary condensation, with methane PMO showing the largest one. This sharp decrease in methane PMO thickness is about 10% of its original thickness, and it corresponds to an abnormally high refractive index near the end of pore condensation, even higher than the refractive index at maximum relative humidity. This peculiar feature of methane PMO suggests an *elastic* character in its mechanical response. A similar feature is also discernible in ethane PMO, albeit less pronounced.

Water Repellent PMOs. To investigate the effect of thermal post-treatment on the hydrophobicity, we performed EP measurements on PMO thin films post-treated at increasing temperatures. Figure 4 shows the isotherms of four PMOs treated at 300 °C, 400 °C, and 500 °C. For all four PMOs, pore condensation shifts to higher relative humidity with increasing temperatures. These shifts indicate that the pore surface becomes progressively more hydrophobic as the temperature of thermal post-treatment increases. At 500 °C, methane and 3-ring PMOs show no pore condensation, which suggests a contact angle equal to or greater than 90°. The chemical nature of this hydrophobization has been reported previously:[18−20] In brief, at temperatures equal or greater than 400 °C, trace amount of silanol groups at the vicinity of bridging organic groups are eliminated by transforming into Si−O−Si bonds and producing terminal organic groups.

The porosities of these water repellent PMOs still remain after the thermal post-treatment, indicating that the porous structure is not collapsed. The refractive indexes at 633 nm of the samples treated at 500 °C are 1.2244 for methane PMO and 1.2445 for 3-ring PMO, which correspond to a porosity of 51% and 46%, respectively.

To demonstrate the accessibility of these pores, spectroscopic ellipsometric measurements were performed on these samples in an atmosphere saturated with ethanol vapor. Ethanol wets the pore wall perfectly, so pore condensation occurs in all accessible pores. The refractive indexes at 633 nm measured under this condition are 1.4240 for methane PMO and 1.4449 for 3-ring PMO, which correspond to a porosity of 51% and 50%, respectively, indicating that all pores are still accessible. The slightly higher porosities obtained from the measurements under ethanol vapor can be attributed to the small amount of ethanol absorbed at the surface of the thin film. In these

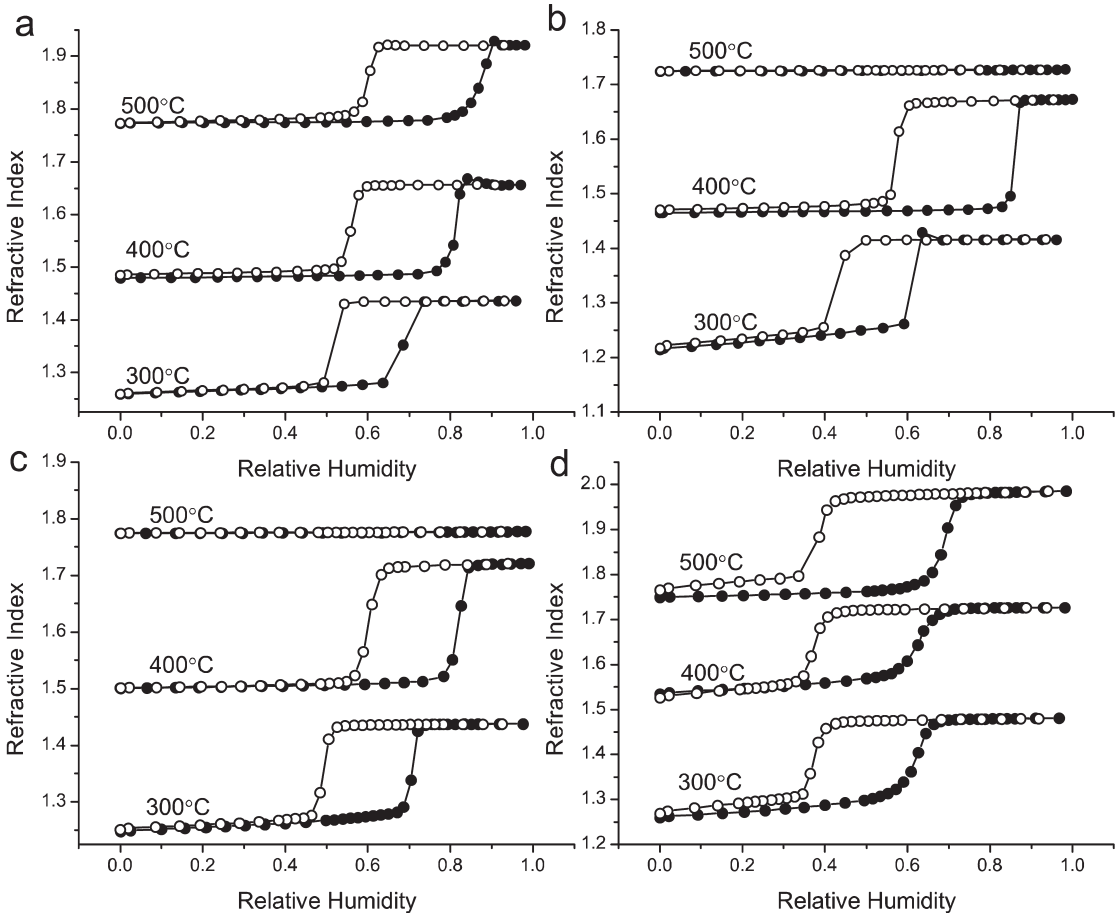

Figure 4. Isotherms of (a) ethane, (b) methane, (c) 3-ring, and (d) ethene PMO post-treated at 300, 400, and 500 °C for 2 h. The plots of samples post-treated at 400 and 500 °C are offset by 0.25 and 0.5, respectively. The plot of the 3-ring PMO post-treated at 500 °C is offset by 0.55.

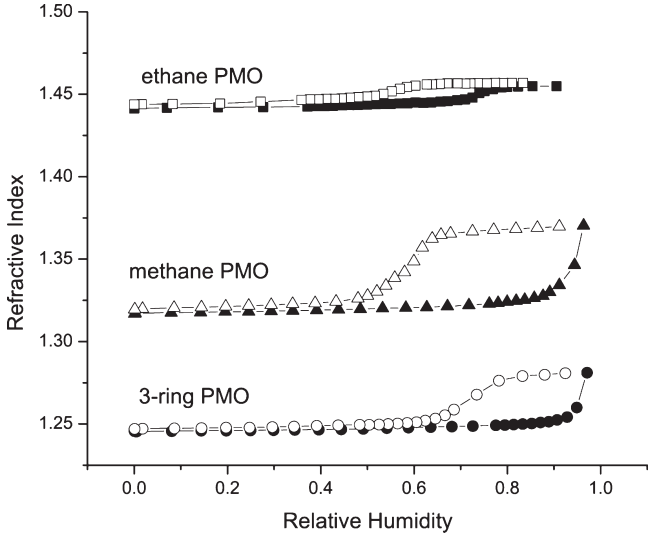

Figure 5. Isotherms of 3-ring, methane, and ethane PMOs post-treated at 350 °C without washing away the templating surfactants. The plot of methane PMO is offset by 0.1, and that of ethane PMO is offset by 0.2.

calculations, the Lorentz–Lorenz equation[21] is used with the assumption that the refractive index of ethanol in confined nanopores is the same as that in the bulk.

Water repellency can also be achieved in ethane, methane, and 3-ring PMOs at lower temperatures if the washing step is skipped and the surfactants are left in the pores. Shown in Figure 5, these films post-treated at 350 °C show little water adsorption before 80% RH, and adsorb only a small amount beyond 80% RH, evidenced by a small increase in the refractive indexes.

TABLE 1. Comparison of Contact Angles Measured Macroscopically on Thin Films of Bridged Polysilsesquioxane and Contact Angles Obtained from EP Measurements on Thin Films of PMOs Post-treated at Temperatures between 300 and 500°C for 2 h[a]

	300 °C	350 °C	400 °C	450 °C	500 °C
$-CH_2CH_2-$ bridged polysilsesquioxane	66.0 ± 0.6	76.1 ± 0.4	82.3 ± 0.2	81.4 ± 0.2	78.0 ± 0.5
ethane PMO	69 ± 2	76 ± 1	79 ± 1	79 ± 1	83 ± 0.5
$-CH_2-$ bridged polysilsesquioxane	55.9 ± 0.4	68.1 ± 0.4	83.4 ± 0.3	93.2 ± 0.2	94.5 ± 0.3
methane PMO	62 ± 2	73 ± 1	82 ± 0.5	>90	>90
3-ring polysilsesquioxane	70.5 ± 0.3	75.9 ± 0.3	82.0 ± 0.5	91.9 ± 0.1	103.6 ± 0.3
3-ring PMO	71 ± 2	80 ± 1	79 ± 1	>90	>90
$-CH=CH-$ bridged polysilsesquioxane	53.2 ± 0.5	61.6 ± 0.2	67.9 ± 0.6	70.2 ± 0.5	62.1 ± 0.2
ethene PMO	63 ± 3	63 ± 3	63 ± 3	65 ± 3	69 ± 2

[a] Standard deviations of macroscopically measured contact angles are obtained from at least six advancing angles on the same sample. Standard deviations of contact angels derived from EP are obtained by propagating the errors in the estimated pore size distributions.

Quantitatively, this increase is 0.03 for 3-ring PMO, 0.05 for methane PMO, and 0.01 for ethane PMO. These values are small compared to an increase of 0.16−0.18 if pore condensation occurs. This enhanced hydrophobicity can be attributed to residual carbon left from the thermal decomposition of surfactants.

On the Validity of Deriving Contact Angles Using the Kelvin Equation. It has been long noted that the very concept of a meniscus, as well as the concept of a contact angle, becomes questionable as the pore size decreases to the width of a few molecules.[22] In thin films of PMOs, the pore size is about 2 nm, which roughly corresponds to the width of 200 water molecules.[23] Although small, this number is sufficient for the formation of a curved surface from a purely geometric point of view. To further investigate this proposition, we measure the macroscopic contact angles on thin films of bridged polysilsesquioxane (nonporous) and compare them with the values derived by applying the Kelvin equation to the adsorption branch of the isotherms. The results are shown in Table 1. The values obtained from the two methods are generally in good agreement with each other, which suggests that the concept of a meniscus, as well as the concept of a contact angle, is still valid in the mesopores.

Quantitative discrepancies are attributed mainly to two assumptions. First, it is assumed that the 2 nm pore size is independent of the temperature of thermal post-treatment and is independent of the type of PMO. This assumption is partially justified because the values of the *d*-spacing vary only slightly below 500 °C post-treatment (Supporting Information Table S1). Also since the template used is the same for all PMOs, the pore size is expected to be around the same value for all PMOs. It is also worth noticing that previous studies[24,25] on thin films of mesoporous silica indicate anisotropic contraction along the out-of-plane direction, so strictly speaking 2 nm is the length of the short axis of a "brick-like" pore. Second, the thickness of the adsorbed water layer is assumed to be zero. The radius term in the Kelvin equation is more accurately described as the radius of a meniscus, and the true radius should be the sum of the radius of the meniscus and the thickness of an adsorbed water layer before pore condensation. The assumption that the thickness of this adsorbed water layer is zero introduces little errors in ethane, methane, and 3-ring PMOs because the slopes of the isotherms before pore condensation are almost flat, indicating little water adsorption before pore condensation. However in ethene PMO, this assumption can introduce significant errors because the observed slopes are not flat. Experimentally, it is difficult to measure the thickness of this absorbed water layer, so for easy comparison and the convenience in discussion, we assume that the adsorbed layer is zero in ethene PMO.

In the preceding discussion, we also tacitly assume that the contact angle is derived by applying the Kelvin equation to the adsorption branch, but not to the desorption branch. However, the existence of hysteresis in all EP isotherms raises the question of why not the latter case. To quantitatively answer this question, it is necessary to take into account different models of hysteresis,[22] the effect of capillary pressure in nanopores on the molar volume of water,[26] the decrease of surface tension in nanometer-sized fluid,[27] and the possible effect of one-dimensional nanopore confinement on the behavior of the phase transition from gas to condensed fluid.[28] Addressing all these issues is out of the scope of this study. Here we only briefly explain our choice from an experimentalist's point of view. First, during an EP measurement, the surface of the pore wall is rehydrolyzed. This rehydrolysis is most likely to occur after pore condensation and before pore evaporation because condensed water is readily available for the reaction. Therefore, the chemical nature of the pore surface reflected by the pore evaporation in desorption branches does not reflect the chemical nature of the pore surface right after thermal treatment. Second, we did not observe a strict 2 to 1 ratio of pore sizes derived from adsorption and desorption branches of the isotherms (Supporting Information Table S2), which should be expected if the model of cylindrical pores with two open ends applies,[22] so the

TABLE 2. Structural and Physical Properties of Four PMOs[a]

name	porosity (*E*) (%)	porosity (EP) (%)	*d*-spacing (Å)	pore diameter (Å)	pore wall thickness (Å)	*E* (SAWS) (GPa)	*E* (EP) (GPa)	*k*
ethane PMO	45 ± 2	45 ± 2	34.8 ± 0.2	20 ± 2	20.4 ± 2	10.2 ± 0.4	2.2 ± 0.4	1.67 ± 0.06
methane PMO	53 ± 2	51 ± 2	35.1 ± 0.4	20 ± 2	20.5 ± 2	10.1 ± 0.9	2.3 ± 0.2	1.60 ± 0.03
3-ring PMO	50 ± 2	49 ± 2	38.4 ± 0.7	20 ± 2	24.3 ± 2	14.4 ± 0.4	2.2 ± 0.5	1.63 ± 0.07
ethene PMO	44 ± 2	40 ± 3	35.4 ± 1.4	20 ± 2	20.1 ± 2	9.1 ± 0.5	3.2 ± 0.5	1.70 ± 0.06

[a] Standard deviations (STDs) of porosities (*E*) and (EP), *d*-spacing and *E* (EP) are obtained from values of 4−6 samples. STDs of pore wall thickness are obtained by propagating the errors in estimated pore size. STDs of *k* are obtained from 4−6 pads on one thin film sample. STDs of SAWS are obtained from measurements at six different laser-to-detector distances on one sample.

existence of hysteresis is most likely related to the ink-bottle effect,[22] in which a "neck" having a smaller diameter than the size of a mesopore regulates the flow of vapor in and out of the mesopores. According to this ink-bottle model, pore evaporation in the desorption branch is related to the size of the neck, whereas pore condensation in the adsorption branch is related to the size of the mesopore. This model was used in a previous report,[29] although no justification was given.

Summary of Properties Pertinent to Low-*k* Applications. Key structural, mechanical, and dielectric properties of four PMOs are summarized in Table 2. The difference between Young's moduli obtained by EP and by surface acoustic wave spectroscopy (SAWS) may be attributed to the difference in the out-of-plane and in-plane Young's moduli.[12] Both techniques exclude the effect of a substrate, and SAWS in particular has been the choice for studying Young's modulus of low-*k* thin films in the semiconductor industry.[30−32] It has been pointed out that a Young's modulus (SAWS) higher than 4 GPa is sufficient for a low-*k* material to survive chemical mechanical planarization.[30] Because reducing structural connectivity decreases the Young's modulus of a sol−gel film,[32,33] increasing the degree of polycondensation should better the mechanical properties. The Young's moduli (SAWS) in Table 2 are obtained from template-removed samples heated with a slow ramping rate of 1 °C/min and at 350 °C for 2−6 h (a temperature before self-hydrophobization occurs), so they represent possibly the highest values these PMOs can achieve, higher than the values reported in the literature for films having the same densities (~7 GPa for both ethane and methane PMO[30,31]). In addition, a collective effect of a periodically ordered structure in PMOs may also contribute to the enhanced mechanical properties.

Insights into the hydrophilic−hydrophobic sequence of the four PMOs can help guide the future design of PMO precursors in application areas not limited to low-*k* materials. Here we offer our thoughts from a chemistry perspective. Since silanol groups are most attractive to water molecules, a reduction of the number of silanol groups per unit surface area will increase hydrophobicity. In 3-ring PMO, each silicon atom is bonded to only two oxygen atoms (and thus a maximum of two silanol groups per silicon atom), whereas in the rest of the PMOs each silicon atom is bonded to three oxygen atoms, so 3-ring PMO is expected to have the least number of silanol groups per unit surface area. Moreover, the symmetrical ring-shape of 3-ring PMO removes the contribution of any polarity of Si−C bonds, rendering the overall structure more nonpolar and less attractive to water molecules. Therefore, 3-ring PMO is the most hydrophobic of all four PMOs. A similar argument based on the number of silanol groups per unit surface area can be made on the difference between ethane and methane PMO: Because ethane contains one more carbon in the bridge, it has a slightly lower concentration of silanol groups than methane PMO. In ethene PMO, the electrons of π-bond are more polarizable by the dipoles of water molecules than the σ-bond electrons in the other three PMOs, making ethene PMO more attractive to water molecules. In addition, the precursor of ethene PMO contains both cis and trans isomers, and the cis isomer is expected to contribute additional dipole moment density that attracts water molecules. The double bonds also delocalize the charge of any transition state involved in the rehydrolysis reaction and hence facilitate the rehydrolysis. Overall, ethene PMO is the least hydrophobic of all PMOs.

CONCLUSION

We have demonstrated for the first time the gradual hydrophobization of PMOs and monitored this change quantitatively by ellipsometric porosimetry. In particular, ethane, methane, and 3-ring PMOs show water repellency at post-treatment temperature as low as 350 °C, with corresponding Young's modulus values greater than 10 GPa and *k* values smaller than 2. This combination of dielectric, mechanical, and humidity resistant properties satisfies the immediate demand of the semiconductor industry for low-*k* materials, and we believe these PMOs will play a role in overcoming the major roadblock facing the integration of porous low-*k* materials on semiconductor chips.[34] From the perspective of materials chemistry, by borrowing a tool invented in the semiconductor industry, we demonstrated a materials chemistry approach to the fine-tuning of

hydrophilic and hydrophobic properties of PMOs, and we believe this flexibility in hydrophobization will benefit potential areas of applications beyond the semiconductor industry.

METHODS

Thin Films of PMO. 1,2-Bis(triethoxysilyl))ethane and 1,2-bis-(trimethoxysilyl)ethane (ethane PMO precursor) and cetyltrimethylammonium chloride (CTACl) 25 wt % solution in water were purchased from Aldrich. Bis(triethoxysilyl)methane (methane PMO precursor), 1,1,3,3,5,5-hexaethyoxy-1,3,5-trisilacyclohexane (3-ring PMO precursor), and bis(triethoxysilyl-)ethylene (ethene PMO precursor) were purchased from Gelest. In a typical synthesis, PMO precursor was added into a solution of CTACl, HCl, water, and ethanol with moderate stirring. The molar ratio of the reactants was Si/CTACl/HCl/H_2O/EtOH = 1:0.15:2 $\times$ 10^{-4}:19.1:15 for ethane, methane, and 3-ring PMO, and Si/CTACl/HCl/H_2O/EtOH = 1:0.15:2 $\times$ 10^{-3}: 19.1:15 for ethene PMO. The optimum solution aging time to obtain well-ordered mesostructure (the time from adding precursors to spincoating) was 80−100 min for ethane PMO, 70−90 min for methane PMO, 40−60 min for 3-ring PMO, and 25−40 min for ethene PMO. These as-deposited thin films were heated under nitrogen at 150 °C for 2 h (ramping 1 °C/min) to increase the degree of polycondensation inside the pore wall, before being washed by HCl 10 vol % solution in ethanol to remove surfactants. The thin films were then heated again under nitrogen at a temperature between 300 and 500 °C for 2 h with a ramping rate of 1 °C/min.

Characterization. Low angle X-ray diffraction patterns were collected on a Siemens D5000 diffractometer using Cu Kα radiation operated at 50 KV and 35 mA with a Kevex solid-state detector. Scanning transmission electron microscopy (STEM) imaging was performed on a Hitachi HD-2000 at an acceleration voltage of 200 kV on thin film fragments scratched from the substrate and deposited onto carbon-coated copper grids.

Dielectric constants of the PMO thin films were measured using the parallel plate method at 1 MHz on a 4280A Hewlett-Packard C meter, with the top electrodes being 100 nm-thick gold pads sputtered through a shadow mask on the top of the films, and the bottom electrode being a heavily doped n-type (100) silicon wafer (resistivity: 0.001−0.020 Ω·cm). The area of each gold pad was measured on Olympus PME3 and analyzed by the software Clemex Vision PE 5.0. Thickness of the film was measured by spectroscopic ellipsometry.

Surface acoustic wave spectroscopy measurements were performed on an LAwave system at Fraunhofer USA in Michigan. A nitrogen pulse laser was used to introduce a 500 ps laser pulse focused on a line with a length of about 5 mm. This laser pulse generated a surface acoustic wave package that showed phase velocity dispersion as it propagated along the thin film surface and was detected by a piezoelectric transducer. Phase spectra are obtained by Fourier-transforming the signals and are fitted to theoretical dispersion curve to deduce Young's Modulus. (Poisson's ratio is set to be 0.25.[30])

Ellipsometric porosimetry measurements were performed on a Sopra GES-5E EP-A machine. A thin film was placed inside a chamber where a combination of dry and wet air flow was introduced to vary the relative humidity inside the chamber. Each step of relative humidity was allowed to stabilize for about 30 to 60 s before a spectrum was taken. The spectra were analyzed using the software WinElli from the manufacturer. Contact angles were derived by adjusting the peak of pore size distribution derived from the adsorption branch of the first adsorption−desorption circle to be at 2 nm. The molar volume of water used is 18 mL/mol, and the surface tension of water used is 0.07203 N/m.[35]

Contact angle measurements were performed according to the procedures described in the literature.[36] Briefly, the solid surface was leveled using a bubble level. Water was delivered onto the surface of a thin film through a stainless needle connected to a syringe. The speed of advancing and receding drop front was controlled by a stepper motor connected to the syringe. The drop was illuminated from behind, and the image was taken by a charge-coupled device camera. Contact angles were determined from the images by axisymmetric drop shape analysis-no apex. Advancing angles were used to compare the contact angles derived from EP. Thin films of dense bridged polysilsesquioxane (nonporous) were prepared by dip-coating a solution of PMO precursor, HCl, water, and ethanol or tetrahydrofuran. Films were thermally treated in the same way as thin films of PMOs were.

Acknowledgment. G.A.O. is the Government of Canada Research Chair in Materials Chemistry and Nanochemistry. We thank the Natural Sciences and Engineering Research Council (NSERC) of Canada for financial support of this work, Dr. Srebri Petrov for XRD measurements, Sue Mamiche for sputtering deposition, Kagan Yaran for SAWS measurements, and Ali Kalantarian and Zdenka Policova for their assistance on contact angle measurements.

Supporting Information Available: Tables of (1) *d*-spacing of PMOs post-treated at various temperatures, (2) pore size derived from adsorption and desorption branch, (3) densities and Young's moduli of dense-bridged silsesquioxane (nonporous) film, and (4) densities of PMO film used for SAWS fitting; a figure of the experimental and fitted X-ray reflectivity patterns of dense bridged silsesquioxane (nonporous) film; experimental method of X-ray reflectivity measurements. This material is available free of charge *via* the Internet at http://pubs.acs.org.

REFERENCES AND NOTES

1. Inagaki, S.; Guan, S.; Fukushima, Y.; Ohsuna, T.; Terasaki, O. Novel Mesoporous Materials with a Uniform Distribution of Organic Groups and Inorganic Oxide in Their Frameworks. *J. Am. Chem. Soc.* **1999,** *121*, 9611–9614.
2. Melde, B. J.; Holland, B. T.; Blanford, C. F.; Stein, A. Mesoporous Sieves with Unified Hybrid Inorganic/Organic Frameworks. *Chem. Mater.* **1999,** *11*, 3302–3308.
3. Asefa, T.; MacLachlan, M. J.; Coombs, N.; Ozin, G. A. Periodic Mesoporous Organosilicas with Organic Groups inside the Channel Walls. *Nature* **1999,** *402*, 867–871.
4. Hoffmann, F.; Cornelius, M.; Morell, J.; Froba, M. Silica-Based Mesoporous Organic−Inorganic Hybrid Materials. *Angew. Chem., Int. Ed.* **2006,** *45*, 3216–3251.
5. Hatton, B.; Landskron, K.; Whitnall, W.; Perovic, D.; Ozin, G. A. Past, Present, and Future of Periodic Mesoporous Organosilicas the PMOs. *Acc. Chem. Res.* **2005,** *38*, 305–312.
6. Yang, Q.; Liu, J.; Zhang, L.; Li, C. Functionalized Periodic Mesoporous Organosilicas for Catalysis. *J. Mater. Chem.* **2009,** *19*, 1945–1955.
7. Lin, C. X.; Qiao, S. Z.; Yu, C. Z.; Ismadji, S.; Lu, G. Q. Periodic Mesoporous Silica and Organosilica with Controlled Morphologies as Carriers for Drug Release. *Microporous Mesoporous Mater.* **2009,** *117*, 213–219.
8. Wang, X.; Lu, D.; Austin, R.; Agarwal, A.; Mueller, L. J.; Liu, Z.; Wu, J.; Feng, P. Protein Refolding Assisted by Periodic Mesoporous Organosilicas. *Langmuir* **2007,** *23*, 5735–5739.
9. Rebbin, V.; Schmidt, R.; Fröba, M. Spherical Particles of Phenylene-Bridged Periodic Mesoporous Organosilica for High-Performance Liquid Chromatography. *Angew. Chem., Int. Ed.* **2006,** *45*, 5210–5214.
10. Landskron, K.; Hatton, B. D.; Perovic, D. D.; Ozin, G. A. Periodic Mesoporous Organosilicas Containing Interconnected $[Si(CH_2)]_3$ Rings. *Science* **2003,** *302*, 266–269.
11. Hatton, B. D.; Landskron, K.; Whitnall, W.; Perovic, D. D.; Ozin, G. A. Spin-Coated Periodic Mesoporous Organosilica

Thin Films—Towards a New Generation of Low-Dielectric-Constant Materials. *Adv. Funct. Mater.* **2005,** *15*, 823–829.
12. Wang, W. D.; Grozea, D.; Kim, A.; Perovic, D. D.; Ozin, G. A. Vacuum-Assisted Aerosol Deposition of a Low-Dielectric-Constant Periodic Mesoporous Organosilica Film. *Adv. Mater.* **2010,** *22*, 99–102.
13. Dultsev, F. N.; Baklanov, M. R. Nondestructive Determination of Pore Size Distribution in Thin Films Deposited on Solid Substrates. *Electrochem. Solid-State Lett.* **1999,** *2*, 192–194.
14. Baklanov, M. R.; Mogilnikov, K. P.; Polovinkin, V. G.; Dultsev, F. N. Determination of Pore Size Distribution in Thin Films by Ellipsometric Porosimetry. *J. Vac. Sci. Technol., B* **2000,** *18*, 1385–1391.
15. Mogilnikov, K. P.; Baklanov, M. R. Determination of Young's Modulus of Porous Low-*k* Films by Ellipsometric Porosimetry. *Electrochem. Solid-State Lett.* **2002,** *5*, F29–F31.
16. Boissiere, C.; Grosso, D.; Lepoutre, S.; Nicole, L.; Bruneau, A. B.; Sanchez, C. Porosity and Mechanical Properties of Mesoporous Thin Films Assessed by Environmental Ellipsometric Porosimetry. *Langmuir* **2005,** *21*, 12362–12371.
17. Volksen, W.; Miller, R. D.; Dubois, G. Low Dielectric Constant Materials. *Chem. Rev.* **2010,** *110*, 56–110.
18. Asefa, T.; MacLachlan, M. J.; Grondey, H.; Coombs, N.; Ozin, G. A. Metamorphic Channels in Periodic Mesoporous Methylenesilica. *Angew. Chem., Int. Ed.* **2000,** *39*, 1808–1811.
19. Hatton, B. D.; Landskron, K.; Hunks, W. J.; Bennett, M. R.; Shukaris, D.; Perovic, D. D.; Ozin, G. A. Materials Chemistry for Low-*k* Materials. *Mater. Today* **2006,** *9*, 22–31.
20. Hatton, B. D. Mechanical and Dielectric Properties of Self-Assembled, Periodic Nanoporous Silica and Organosilica Materials. Ph.D. Thesis, University of Toronto, Toronto, 2005.
21. Gerald E. Jellison, J. Data Analysis for Spectroscopic Ellipsometry. In *Handbook of Ellipsometry*; Tompkins, H. G., Irene, E. A., Eds.; William Andrew Publishing and Springer-Verlag GmbH & Co. KG: Norwich and Heidelberg, 2005.
22. Gregg, S. J.; Sing, K. S. W. *Adsorption, Surface Area, and Porosity*; 2nd ed.; Academic Press: London, 1982.
23. Lu, H. M.; Jiang, Q. Size-Dependent Surface Tension and Tolman's Length of Droplets. *Langmuir* **2005,** *21*, 779–781.
24. Yang, H.; Kuperman, A.; Coombs, N.; Mamiche-Afara, S.; Ozin, G. A. Synthesis of Oriented Films of Mesoporous Silica on Mica. *Nature* **1996,** *379*, 703–705.
25. Klotz, M.; Albouy, P. A.; Ayral, A.; Menager, C.; Grosso, D.; Van der Lee, A.; Cabuil, V.; Babonneau, F.; Guizard, C. The True Structure of Hexagonal Mesophase-Templated Silica Films as Revealed by X-Ray Scattering: Effects of Thermal Treatments and of Nanoparticle Seeding. *Chem. Mater.* **2000,** *12*, 1721–1728.
26. Bridgman, P. W. The Pressure−Volume−Temperature Relations of the Liquid, and the Phase Diagram of Heavy Water. *J. Chem. Phys.* **1935,** *3*, 597–605.
27. Tolman, R. C. The Effect of Droplet Size on Surface Tension. *J. Chem. Phys.* **1949,** *17*, 333–337.
28. Neimark, A. V.; Ravikovitch, P. I. Capillary Condensation in MMS and Pore Structure Characterization. *Microporous Mesoporous Mater* **2001,** *44*−*45*, 697–707.
29. Kuemmel, M.; Grosso, D.; Boissière, C.; Smarsly, B.; Brezesinski, T.; Albouy, P. A.; Amenitsch, H.; Sanchez, C. Thermally Stable Nanocrystalline γ-Alumina Layers with Highly Ordered 3D Mesoporosity. *Angew. Chem., Int. Ed.* **2005,** *44*, 4589–4592.
30. Dubois, G.; Volksen, W.; Magbitang, T.; Miller, R. D.; Gage, D. M.; Dauskardt, R. H. Molecular Network Reinforcement of Sol−Gel Glasses. *Adv. Mater.* **2007,** *19*, 3989–3994.
31. Dubois, G.; Volksen, W.; Magbitang, T.; Sherwood, M. H.; Miller, R. D.; Gage, D. M.; Dauskardt, R. H. Superior Mechanical Properties of Dense and Porous Organic/Inorganic Hybrid Thin Films. *J. Sol−Gel Sci. Technol.* **2008,** *48*, 187–193.
32. Oliver, M. S.; Dubois, G.; Sherwood, M.; Gage, D. M.; Dauskardt, R. H. Molecular Origins of the Mechanical Behavior of Hybrid Glasses. *Adv. Funct. Mater.* **2010,** *20*, 2884–2892.
33. Ro, H. W.; Char, K.; Jeon, E. C.; Kim, H. J.; Kwon, D.; Lee, H. J.; Lee, J. K.; Rhee, H. W.; Soles, C. L.; Yoon, D. Y. High-Modulus Spin-on Organosilicate Glasses for Nanoporous Applications. *Adv. Mater.* **2007,** *19*, 705–710.
34. *International Technology Roadmap for Semiconductors*; Interconnect, 2009.
35. Kayser, W. V. Temperature Dependence of the Surface Tension of Water in Contact with Its Saturated Vapor. *J. Colloid Interface Sci.* **1976,** *56*, 622–627.
36. Kalantarian, A.; David, R.; Neumann, A. W. Methodology for High Accuracy Contact Angle Measurement. *Langmuir* **2009,** *25*, 14146–14154.